SCIENTIFIC REPORTS

OPEN

SUBJECT AREAS:
ELECTRONIC DEVICES
SURFACES, INTERFACES AND THIN FILMS

Received
7 May 2014

Accepted
8 July 2014

Published
24 July 2014

Correspondence and requests for materials should be addressed to H.T. (h-tanaka@sanken.osaka-u.ac.jp)

Dual field effects in electrolyte-gated spinel ferrite: electrostatic carrier doping and redox reactions

Takashi Ichimura, Kohei Fujiwara & Hidekazu Tanaka

The Institute of Scientific and Industrial Research, Osaka University, Ibaraki, Osaka 567-0047, Japan.

Controlling the electronic properties of functional oxide materials via external electric fields has attracted increasing attention as a key technology for next-generation electronics. For transition-metal oxides with metallic carrier densities, the electric-field effect with ionic liquid electrolytes has been widely used because of the enormous carrier doping capabilities. The gate-induced redox reactions revealed by recent investigations have, however, highlighted the complex nature of the electric-field effect. Here, we use the gate-induced conductance modulation of spinel $Zn_xFe_{3-x}O_4$ to demonstrate the dual contributions of volatile and non-volatile field effects arising from electronic carrier doping and redox reactions. These two contributions are found to change in opposite senses depending on the Zn content x; virtual electronic and chemical field effects are observed at appropriate Zn compositions. The tuning of field-effect characteristics via composition engineering should be extremely useful for fabricating high-performance oxide field-effect devices.

The electric-field effect with a field-effect transistor structure is a powerful approach for externally tuning the carrier density of a material and investigating the associated changes in electronic properties[1]. In the past decade, significant progress has been made in field-effect experiments for functional transition-metal oxides such as high-T_c cuprates and colossal magnetoresistive manganites. In particular, the field effect with ionic liquid electrolytes demonstrating field-induced superconductivity[2,3] and carrier-induced ferromagnetism[4] in insulators, in addition to electronic phase switching in strongly electron correlated systems[5–14], has furthered this field. This method is characterized by an ultrathin capacitor-like structure formed by electrolyte ions at the electrolyte/oxide interface, called the electric double layer (EDL)[15]. The very strong electric field generated within the EDL makes it possible to accumulate a high density of charge carriers on the oxide channel (as high as 10^{14-15} cm^{-2}), without being restricted by the hetero-structuring processes generally required for experiments with solid gate dielectrics. Because functional transition-metal oxides often have metallic carrier densities, EDL gating is widely used as the most effective means for modifying the electronic properties of functional transition-metal oxides.

EDL gating effects in transition-metal oxides have so far been interpreted mainly in terms of electrostatic carrier doping, as in conventional semiconductor field-effect transistors. Recent studies of EDL devices with VO_2[16,17], $SmNiO_3$[18,19], spinel $Zn_xFe_{3-x}O_4$[20] and so on[21,22] have, however, revealed the role of gate-induced redox reactions. Indeed, the electric field produced by EDL gating can be as high as 10 MV cm^{-1}, sufficiently strong to cause motions of constituent atoms/ions and vacancies in those oxides. Those chemical contributions can be identified as non-volatile (persistent) changes in transport properties induced by gate-electric bias (V_G), which cannot be explained by the volatile electrostatic effect. Whether or not the electronic and chemical field effects contradict each other and how the dominant field effect can be controlled in a given material are not yet clear. Here, we demonstrate the coexistence of the two distinct field effects in electrolyte-gated spinel $Zn_xFe_{3-x}O_4$. By varying the Zn substitution level x, we find that the dominant field-effect contribution can be controlled to be either virtually electronic or chemical. The significant role played by composition that has not yet been reported to date would be a new approach to fabricating oxide EDL devices with desirable properties.

Results

Device structure. We fabricated EDL devices with epitaxial thin films of spinel $Zn_xFe_{3-x}O_4$[23,24] grown on single-crystal (001) MgO substrates by pulsed-laser deposition[25], shown in Fig. 1(a) (see the Methods section). Films with nominal Zn contents (x) of 0, 0.5, and 0.8 were used. Cross-sectional transmission electron microscopy observations, shown in Fig. 1(b), confirmed the coherent interface structure with an epitaxial orientation of

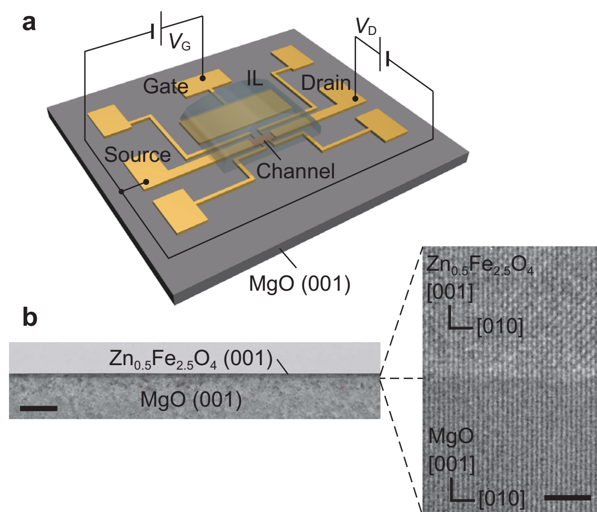

Figure 1 | Electric double-layer device with a spinel ferrite channel. (a), Schematic structure of the device. The $Zn_xFe_{3-x}O_4$ channel is connected to Au/Ti metal electrodes for electrical measurements. IL denotes the ionic liquid electrolyte. (b), Cross-sectional transmission electron microscopy images of a $Zn_{0.5}Fe_{2.5}O_4$ film on a (001) MgO substrate (left; scale bar, 100 nm) and an enlarged view of the interface region (right; scale bar, 2 nm).

(001)[100]$Zn_xFe_{3-x}O_4$||(001)[100]MgO. The device consisted of a Hall-bar-shaped channel with Au/Ti source, drain, and potential probe electrodes and a separate side gate electrode (Fig. 1(a)). The channel length L and width W were 100 µm and 30 µm, respectively, and the thickness was controlled to be between 6 and 7 nm. The EDL capacitor was formed between the channel and gate electrode by bridging them with an ionic liquid electrolyte, N,N-diethyl-N-(2-methoxyethyl)-N-methylammonium bis-trifluoromethylsulfonyl)-imide.

EDL gating effect on conductivity. The Zn content x was sensitively reflected in the electrical conductivity. We measured the drain current (I_D) as a function of V_G with a constant drain voltage (V_D) at 300 K, using the setup shown in Fig. 1(a). V_G was scanned at a rate of 3.3 mV s^{-1} (see Supplementary Note 1 and Fig. S1 for the scan-rate dependence). Figure 2 summarizes channel conductance $G = I_D/V_D$ versus V_G plots (transfer characteristics) for the $Zn_xFe_{3-x}O_4$ EDL devices with different levels of x. Zn^{2+} ions are substituted for Fe^{3+} ions in the spinel A-sites[24]; for the sake of charge neutrality, Fe^{2+} ions in the B-sites that supply t_{2g} electron carriers are converted into Fe^{3+} ions, resulting in a decrease in carrier density and conductivity. The systematic decrease in G with increasing x is consistent with results previously reported for bare thin films[23,24], indicating that our $Zn_xFe_{3-x}O_4$ channels were not degraded by the fabrication procedure.

In Fig. 2, it is commonly observed that the application of a positive (negative) V_G induces an increase (a decrease) in G. Recently we reported that the large G–V_G hysteresis and the bi-stable, non-volatile conductance states at $V_G = 0$ were induced in the $Zn_{0.5}Fe_{2.5}O_4$ EDL device by polarity-dependent reversible changes in the oxygen content by EDL gating[20]. Electric-field-induced oxygen diffusion/migration[21] promoted by the extremely strong electric field of the EDL might be of microscopic origin. Similar features observed in the Fe_3O_4 device indicate that the underlying mechanism for the conductance change is essentially identical to that in the $Zn_{0.5}Fe_{2.5}O_4$ device. However, we observed a noticeable difference between these lightly substituted systems and $Zn_{0.8}Fe_{2.2}O_4$ with regard to hysteresis behaviour. For the former cases, the application of a positive or negative V_G, respectively, induces non-volatile high-G and low-G

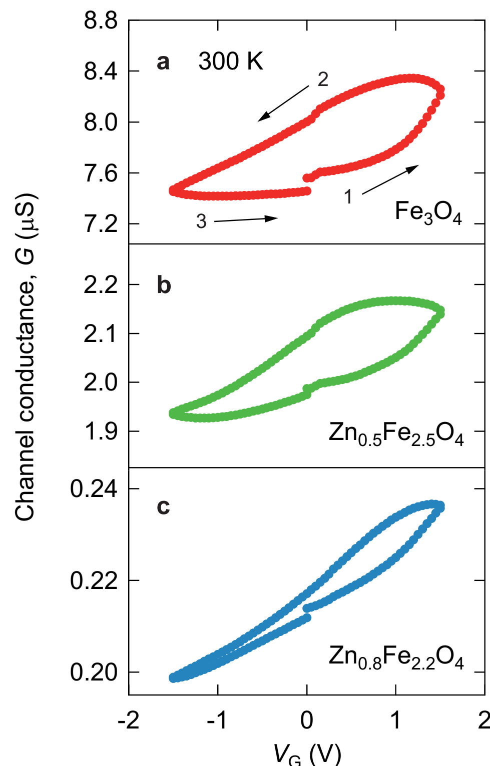

Figure 2 | Gate-induced change in the channel conductance. (a–c), V_G dependencies of $G(=I_D/V_D)$ were measured for the devices fabricated with the $Zn_xFe_{3-x}O_4$ films of $x = 0$ (a), 0.5 (b), and 0.8 (c). For all devices, V_G was scanned in the numerical order shown in (a).

states at $V_G = 0$ (Fig. 2(a) and (b)), whereas for $Zn_{0.8}Fe_{2.2}O_4$ there is only a slight difference in G at $V_G = 0$ (Fig. 2(c)) and the characteristic hysteresis virtually disappears. It suggests that the non-volatile contribution becomes weaker for the $Zn_{0.8}Fe_{2.2}O_4$ device as compared with the other contribution(s). In fact, the almost-linear G–V_G behaviour is rather similar to the properties of $Zn_xFe_{3-x}O_4$ field-effect devices fabricated with a solid gate dielectric[25], in which electrostatic carrier doping is responsible for the field effect. These observations revealed the coexistence of two types of field effects in the $Zn_xFe_{3-x}O_4$ EDL devices and their compositional dependencies.

Compositional dependence. With the aim of separately tracking the evolution of non-volatile and volatile contributions with changes in x, we extracted the corresponding components from the G–V_G curves. Our procedure is depicted schematically in Fig. 3(a). First, the change in G due to the non-volatile field effect, ΔG_{nonvol}, was given by the difference between high and low Gs at $V_G = 0$ V induced by a positive and negative gating, respectively. The remaining change in G, given by $\Delta G_{total} - \Delta G_{nonvol}$, where ΔG_{total} is the total change in G between $V_G = +1.5$ and -1.5 V, was then defined as the contribution from the volatile field effect. To compare those devices with different G values, ΔG_{total}, ΔG_{nonvol}, and ΔG_{vol} were scaled to the base G values measured at $V_G = 0$ V after the negative gating cycle, G_0^{low}, as shown in Fig. 3(a).

We present in Fig. 3(b) the normalized values of ΔG_{total}, ΔG_{nonvol}, and ΔG_{vol} plotted versus x, where their contrasting dependencies on x can be clearly seen. For the Fe_3O_4 ($x = 0$) and $Zn_{0.5}Fe_{2.5}O_4$ ($x = 0.5$) EDL devices, ΔG_{nonvol} is as large as 7–8%, which is approximately twice ΔG_{vol} (3–5%). Consequently, in low-x devices, the non-volatile contribution occupies a significant part of the conductance modulation (~70%). A further increase in x drastically alters the field-effect mode; in the $Zn_{0.8}Fe_{2.2}O_4$ ($x = 0.8$) EDL devices, the non-volatile contribution in turn becomes as small as 3.5% and the volatile contribution rapidly increases up to ~12.5%.

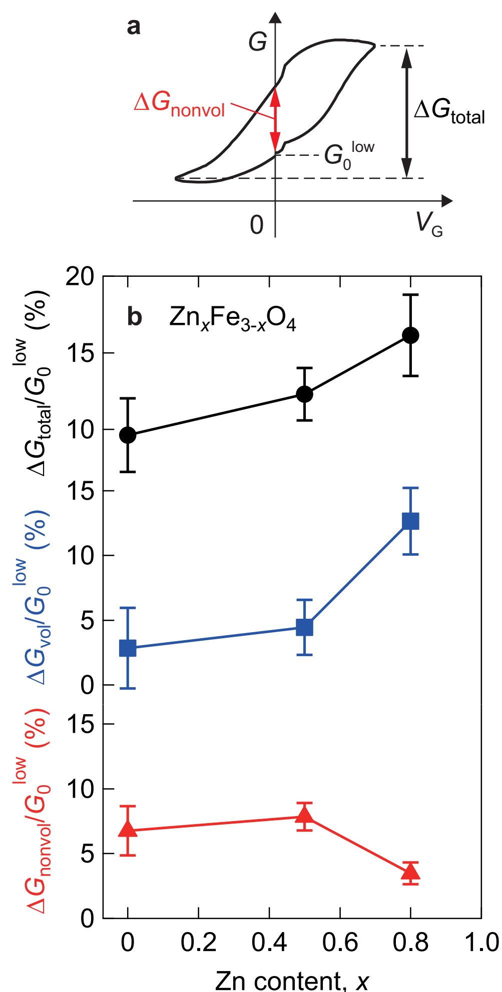

Figure 3 | Evolution of non-volatile and volatile conductance changes with Zn substitution. (a), The definition of non-volatile contribution (ΔG_{nonvol}) to the total conductance change (ΔG_{total}) is shown schematically. (b), ΔG_{total}, ΔG_{vol}, and ΔG_{nonvol} plotted versus x. The error bars represent the standard deviations of the measured data.

Discussion

We first consider the origin of the volatile contribution ΔG_{vol}. Spinel Zn ferrites have been reported to have metallic carrier densities in the range of x investigated in the present work[23]. Even in such metallic systems, because of the large capacitance of EDL (typically as large as 1–10 μF cm^{-2}), electrostatic carrier doping should affect G when V_G is applied. Because it is difficult to anticipate the presence of chemical reactions that do not leave any trace after the removal of V_G, electrostatic carrier doping is thought to be the origin of the volatile field effect. Indeed, the observed ΔG_{vol} was explained by electrostatic carrier doping and the x-dependent bulk carrier density n_{bulk}. The introduction of Zn^{2+} ions into the A-sites of spinel Fe_3O_4 reduces n_{bulk}, as mentioned above[23,24]. The number of charge carriers that can be externally modulated by electrostatic carrier doping, n_{FE}, is determined by the capacitance of EDL and the applied V_G, which should remain unchanged irrespective of x for the present case. Electrostatic carrier doping is therefore expected to be strong with increasing n_{FE}/n_{bulk} and hence $1/n_{bulk}$. In Fig. 4, $1/n_{bulk}$ is plotted as a function of x. The carrier density extracted from the ordinal Hall term of the anomalous Hall effect at 300 K[23] was used as n_{bulk}. One can see that this plot reproduces well the experimental trend of ΔG_{vol} (Fig. 3(b)). The increase in ΔG_{vol} as x increases from 0 to 0.5 is a factor of ~1.5, which is less than the change in $1/n_{bulk}$. This is because of the variation in mobility in the low-x regime (see Supplementary Fig. S2); the reduction in mobility suppresses the enhancement in G. The effective enhancement in G taking n_{bulk} and mobility contributions into account is a factor of ~1.2, very close to the increase in ΔG_{vol} observed. Note here that the mobility variation does not play an essential role in the evolution of ΔG_{vol}. In the high-x regime where mobility saturates (Supplementary Fig. S2), the increase in ΔG_{vol} as x increases from 0.5 to 0.8 is a factor of ~2.8, which is in excellent agreement with the change in $1/n_{bulk}$ of ~2.7. These correlations between ΔG_{vol} and $1/n_{bulk}$ support that the volatile field effect observed in our devices originates from the electrostatic carrier doping effect.

Evidence for the almost electrostatic operation in the high-x $Zn_{0.8}Fe_{2.2}O_4$ EDL device was obtained by field-effect mobility μ_{FE} calculations. Based on the slope of the $G(=I_D/V_D) - V_G$ curve (Fig. 2(c)), μ_{FE} was estimated to be 3–5 × 10^{-3} cm^2 V^{-1} s^{-1} using the general relation: $\mu_{FE} = \frac{\partial I_D}{\partial V_G}\left(\frac{L}{CWV_D}\right)$, where C is the capacitance per unit area of the ionic liquid. We adopted a typical C value of 10 μF cm^{-2} from the literature[26]. The μ_{FE} value agrees well with the independently measured value for $Zn_{0.8}Fe_{2.2}O_4$ field-effect transistors with a solid parylene gate dielectric exhibiting n-type field-effect behaviour (μ_{FE} = 4.0 × 10^{-3} cm^2 V^{-1} s^{-1}). On the basis of these results, it is reasonable to consider that the high-x EDL devices are located on the extension of the conventional solid gate dielectric-based field-effect transistors. The contribution of electrostatic carrier doping is thus effectively modulated by varying x and the subsequent changes in n_{bulk}.

The G–V_G hysteresis becomes obvious with decreasing x and weakening electrostatic carrier doping owing to the relatively enhanced non-volatile contribution ΔG_{nonvol}. One interesting point that should be noted from Fig. 3(b) is that ΔG_{nonvol} also shows a dependence on x. Although the microscopic redox mechanism responsible for the non-volatile field effect has not yet been fully understood, we can provide the following tentative explanation based on a previously proposed picture in which we speculated that electric-field-induced oxygen diffusion was the root of the redox[20]. In systems with metallic carrier densities, charge carriers accumulate in the limited thickness of the channel owing to the short screening length L_s, giving rise to a steep potential gradient, i.e., electric field, at the electrolyte/oxide interface. The interfacial electric field is considered to have a characteristic depth profile; its detailed function remains to be determined. Instead, we here assume that the electric-field strength scales roughly inversely with L_s, and use $1/L_s$ as an index of the relative strength. In Fig. 4, $1/L_s$ is plotted versus x. L_s was deduced using the typical relative dielectric constant of conduct-

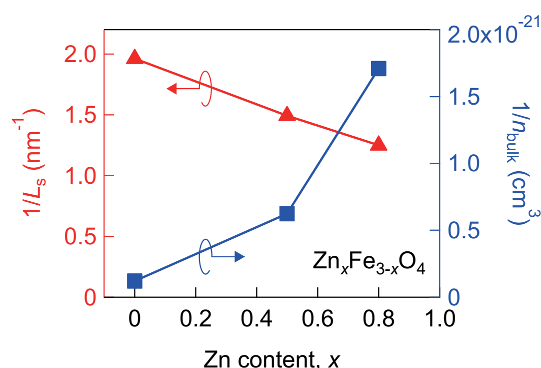

Figure 4 | Variations in bulk carrier density and electronic screening length versus x. The values of n_{bulk} were deduced from the anomalous Hall effect[23]. An external magnetic field of up to 9 T was applied perpendicular to the film plane and the transverse Hall voltage was measured by a voltmeter. The electronic screening length was calculated using the estimated n_{bulk} based on Thomas-Fermi screening.

ive ferrites from the literature[27,28] and n_{bulk}, based on Thomas-Fermi screening. This plot mimics the overall trend of ΔG_{nonvol} (Fig. 3(b)), in that both L_s and ΔG_{nonvol} slowly decrease with increasing x. The suppression of ΔG_{nonvol} in the high-x regime can be understood as being due to the increased L_s and the resulting reduction in the interfacial electric field. To get additional insight into the redox origin and the correlation between L_s and ΔG_{nonvol}, a system exhibiting much larger ΔG_{nonvol} should be identified. Such a discovery would allow one to evaluate the compositional dependence much more quantitatively. Materials with high oxygen diffusion constants and high carrier densities, such as fuel cell electrode materials, may be interesting targets for addressing these issues.

In parallel with the progress of oxide field-effect devices, the oxide research community has recently produced a new type of non-volatile memory element called the resistive switching device[29–31]. The device structure consists of a metal/oxide/metal stack; by applying an electric-field bias between the two metal electrodes, non-volatile electrical resistance switching can be induced. Although the detailed switching mechanism depends on the physical and chemical properties of the oxide medium and the device geometry employed, it is widely accepted that redox reactions such as metal cation and/or oxygen anion diffusion promoted by strong electric field and/or current density play crucial roles[32]. So far, oxide field-effect devices, which are, in principle, based on purely electronic effects, have been categorized as a different class of devices from redox-based switching devices. In the light of the similarities between the non-volatile field effect in EDL devices and the resistive switching effect, however, non-volatile EDL devices may be regarded as a three-terminal analogue of resistive switching devices. At this point, we may have opportunities to fabricate high-performance (e.g., large on/off ratio, fast switching speed), non-volatile EDL devices by using insights accumulated from research of resistive switching devices.

Another feature commonly observed in EDL devices and resistive switching devices is the influence of environment, i.e., surrounding atmosphere, on electrical properties[33]. The presence of oxygen and/or water in the ionic liquid electrolyte was reported to affect EDL gating behaviour[16,17,19,22]. Given electric-field-induced oxygen diffusion/migration as the mechanism of the gate-induced non-volatile conductance, such environment effects might be more clearly observed in materials with high oxygen diffusion constants such as rutile[16,17,22] and perovskite compounds[18,19] than in spinels.

In summary, in spinel $Zn_xFe_{3-x}O_4$ gated with an ionic liquid electrolyte, we revealed the dual contributions of non-volatile and volatile field effects to gate-induced conductance modulation and their dependencies on x. The control of the dominant field-effect mode via a simple composition variation demonstrated here should work for a variety of transition-metal oxides and hence be important for exploring their exotic electronic states with EDL gatings, as well as fabricating oxide EDL devices with specifically designed properties.

Methods

Film growth. Epitaxial thin films of $Zn_xFe_{3-x}O_4$ were grown on (001) surfaces of MgO substrates by pulsed-laser deposition using an ArF excimer laser. Prior to deposition, the MgO substrates were annealed at 700°C using an oxygen pressure of 1 atm to obtain atomically smooth surfaces[34]. The film deposition was performed at 400°C in an oxygen pressure of 1×10^{-4} Pa. The thicknesses of the films were evaluated by atomic force microscopy.

Device fabrication. The films were patterned into a Hall-bar-shaped channel by photolithography and Ar ion milling. The electrodes were prepared using an electron-beam-deposited bilayer film of 50-nm-thick Au and 5-nm-thick Ti. The other device surfaces were covered with a 30-nm-thick SiO_2 film by radio-frequency sputtering (not depicted in Fig. 1(a)) to form an EDL capacitor structure only between the channel and gate electrode. After dropping a small amount of the ionic liquid electrolyte on the channel area, the devices were evacuated to a high vacuum ($\sim 5 \times 10^{-5}$ Pa) to remove contaminations that could possibly exist in the ionic liquid. The devices were then immediately loaded into a Quantum Design Physical Property Measurement System.

Electrical measurements. Transfer characteristics were measured at 300 K using a Keithley 2612A SourceMeter and a 6482 Picoammeter. A V_D of 0.1 V was applied for $x = 0$ and 0.5; a V_D of 0.25 V was applied for $x = 0.8$. The gate leakage current in the V_G range measured was less than 0.5 nA, which was negligibly small compared with the gate-induced change in I_D.

1. Ahn, C. H. *et al.* Electrostatic modification of novel materials. *Rev. Mod. Phys.* **78**, 1185–1212 (2006).
2. Ueno, K. *et al.* Electric-field-induced superconductivity in an insulator. *Nat. Mater.* **7**, 855–858 (2008).
3. Ueno, K. *et al.* Discovery of superconductivity in $KTaO_3$ by electrostatic carrier doping. *Nat. Nanotechnol.* **6**, 408–412 (2011).
4. Yamada, Y. *et al.* Electrically induced ferromagnetism at room temperature in cobalt-doped titanium dioxide. *Science* **332**, 1065–1067 (2011).
5. Nakano, M. *et al.* Collective bulk carrier delocalization driven by electrostatic surface charge accumulation. *Nature* **487**, 459–462 (2012).
6. Liu, K. *et al.* Dense electron system from gate-controlled surface metal-insulator transition. *Nano Lett.* **12**, 6272–6277 (2012).
7. Zhou, Y. & Ramanathan, S. Relaxation dynamics of ionic liquid—VO_2 interfaces and influence in electric double-layer transistors. *J. Appl. Phys.* **111**, 084508 (2012).
8. Xiang, P.-H. *et al.* Electrolyte-gated $SmCoO_3$ thin-film transistors exhibiting thickness-dependent large switching ratio at room temperature. *Adv. Mater.* **25**, 2158–2161 (2013).
9. Hatano, T. *et al.* Gate control of electronic phases in a quarter-filled manganite. *Sci. Rep.* **3**, 2904 (2013).
10. Lourembam, J., Wu, J., Ding, J., Lin, W. & Wu, T. Electric field tuning of phase separation in manganite thin films. *Phys. Rev. B* **89**, 014425 (2014).
11. Asanuma, S. *et al.* Tuning of the metal-insulator transition in electrolyte-gated $NdNiO_3$ thin films. *Appl. Phys. Lett.* **97**, 142110 (2010).
12. Scherwitzl, R., Zubko, P., Lichtensteiger, C. & Triscone, J.-M. Electric-field tuning of the metal-insulator transition in ultrathin films of $LaNiO_3$. *Appl. Phys. Lett.* **95**, 222114 (2009).
13. Garcia-Barriocanal, J. *et al.* Electronically driven superconductor-insulator transition in electrostatically doped $La_2CuO_{4+\delta}$ thin films. *Phys. Rev. B* **87**, 024509 (2013).
14. Dubuis, G., Bollinger, A. T., Pavuna, D. & Božović, I. Electric field effect on superconductivity in $La_{2-x}Sr_xCuO_4$. *J. Appl. Phys.* **111**, 112632 (2012).
15. Ueno, K. Electric-field-induced superconductivity on an organic/oxide interface. *Jpn. J. Appl. Phys.* **52**, 110129 (2013).
16. Jeong, J. *et al.* Suppresion of metal-insulaor transition in VO_2 by electric field-induced oxygen vacanvy formation. *Science* **339**, 1402–1405 (2013).
17. Ji, H., Wei, J. & Natelson, D. Modulation of the electrical properties of VO_2 nanobeams using an ionic liquid as a gating medium. *Nano Lett.* **12**, 2988–2992 (2012).
18. Shi, J., Ha, S. D., Zhou, Y., Schoofs, F. & Ramanathan, S. A correlated nickelate synaptic transistor. *Nat. Commun.* **4**, 2676 (2013).
19. Ha, S. D., Vetter, U., Shi, J. & Ramanathan, S. Electrostatic gating of metallic and insulating phases in $SmNiO_3$ ultrathin films. *Appl. Phys. Lett.* **102**, 183102 (2013).
20. Fujiwara, K., Ichimura, T. & Tanaka, H. Nonvolatile transport states in ferrite thin films induced by field-effect involving redox processes. *Adv. Mater. Interfaces* **1**, 1300108 (2014).
21. Li, M. *et al.* Suppression of ionic liquid gate-induced metallization of $SrTiO_3$(001) by oxygen. *Nano Lett.* **13**, 4675–4678 (2013).
22. Schladt, T. D. *et al.* Crystal-facet-dependent metallization in electrolyte-gated rutile TiO_2 single crystals. *ACS Nano* **7**, 8074–8081 (2013).
23. Takaobushi, J. *et al.* $Fe_{3-x}Zn_xO_4$ thin film as tunable high Curie temperature ferromagnetic semiconductor. *Appl. Phys. Lett.* **89**, 242507 (2006).
24. Venkateshvaran, D. *et al.* Epitaxial $Zn_xFe_{3-x}O_4$ thin films: a spintronic material with tunable electrical and magnetic properties. *Phys. Rev. B* **79**, 134405 (2009).
25. Ichimura, T., Fujiwara, K., Kushizaki, T., Kanki, T. & Tanaka, H. Unstrained epitaxial Zn-substituted Fe_3O_4 films for ferromagnetic field-effect transistors. *Jpn. J. Appl. Phys.* **52**, 068002 (2013).
26. Ye, J. T. *et al.* Superconducting dome in a gate-tuned band insulator. *Science* **338**, 1193–1196 (2012).
27. Hotta, M., Hayashi, M., Nishikata, A. & Nagata, K. Complex permittivity and permeability of SiO_2 and Fe_3O_4 powders in microwave frequency range between 0.2 and 13.5 GHz. *ISIJ Int.* **49**, 1443–1448 (2009).
28. Peelamedu, R., Grimes, C., Agrawal, D., Roy, R. & Yadoji, P. Ultralow dielectric constant nickel–zinc ferrites using microwave sintering. *J. Mater. Res.* **18**, 2292–2295 (2011).
29. Sawa, A. Resistive switching in transition metal oxides. *Mater. Today* **11**, 28–36 (2008).
30. Waser, R., Dittmann, R., Staikov, G. & Szot, K. Redox-based resistive switching memories — nanoionic mechanisms, prospects, and challenges. *Adv. Mater.* **21**, 2632–2663 (2009).
31. Jeong, D. S. *et al.* Emerging memories: resistive switching mechanisms and current status. *Rep. Prog. Phys.* **75**, 076502 (2012).
32. Yang, J. J., Inoue, I. H., Mikolajick, T. & Hwang, C. S. Metal oxide memories based on thermochemical and valence change mechanisms. *MRS Bull.* **37**, 131–137 (2012).

33. Nagashima, K. *et al*. Prominent thermodynamical interaction with surroundings on nanoscale memristive switching of metal oxides. *Nano Lett.* **12**, 5684–5690 (2012).
34. Zama, H., Ishii, Y., Yamamoto, H. & Morishita, T. Atomically flat MgO single-crystal surface prepared by oxygen thermal annealing. *Jpn. J. Appl. Phys.* **40**, 465–467 (2001).

Acknowledgments

This work was supported by the Industrial Technology Research Grant Program in 2009 from NEDO, a Grant-in-Aid for Young Scientists (B) (No. 25790041) from JSPS, the Nanotechnology Platform Project (Nanotechnology Open Facilities in Osaka University) of MEXT (No. F-13-OS-0019, S-13-OS-0016), and the Murata Science Foundation, Japan.

Author contributions

K.F. conceived and designed the experiments. T.I. and K.F. fabricated the devices and collected the data. T.I. analyzed the data. All authors discussed the results and co-wrote the manuscript. H.T. supervised the project.

Additional information

Supplementary information accompanies this paper at http://www.nature.com/scientificreports

Competing financial interests: The authors declare no competing financial interests.

How to cite this article: Ichimura, T., Fujiwara, K. & Tanaka, H. Dual field effects in electrolyte-gated spinel ferrite: electrostatic carrier doping and redox reactions. *Sci. Rep.* **4**, 5818; DOI:10.1038/srep05818 (2014).

This work is licensed under a Creative Commons Attribution-NonCommercial-ShareAlike 4.0 International License. The images or other third party material in this article are included in the article's Creative Commons license, unless indicated otherwise in the credit line; if the material is not included under the Creative Commons license, users will need to obtain permission from the license holder in order to reproduce the material. To view a copy of this license, visit http://creativecommons.org/licenses/by-nc-sa/4.0/